Supporting Information for "Vertical Land Motion from present-day deglaciation in the wider Arctic"

Carsten Ankjær Ludwigsen[1], Shfaqat Abbas Khan[1], Ben Marzeion[2]and Ole Baltazar Andersen[1]

[1]DTU Space, Technical University of Denmark
[2]Institute of Geography and MARUM – Center for Marine Environmental Sciences, University of Bremen, Germany

Contents of this file

1. S1 - Description of glacier ice model
2. S2 - Detailed description of the VLM signal at GNSS-site
3. S3 - Timeseries of vertical deformation at GNSS sites

S1 Description of glacier ice model

As initial conditions, we use glacier outlines obtained from RGI 6.0 (Pfeffer et al., 2014). The time stamp of these outlines differs between glaciers, but is typically around the year 2000. To obtain results before this time, the model uses an iterative process to find the glacier geometry in the year of initialization (e.g., 1901) that results in the observed glacier geometry in the year of the outline's time stamp (e.g., 2000) after the model was run forward.

The model relies on monthly temperature and precipitation anomalies to calculate the specific mass balance of each glacier. Here, we use the mean of seven different reanalysis products as boundary conditions. Temperature is used to estimate the ablation of glaciers following a temperature-index melt model, and to estimate the solid fraction of total precipitation, which is used to estimate accumulation.

Mass balance data for each glacier is distributed over the glacier according to a mathematical approximation, assuming conservation of mass and that the glacier has a elevation gain at the top which becomes a elevation decline further down the glacier. The altitude where the elevation change goes from positive to negative, E, is approximated by a simple function of the glacial altitude (Z) and the averaged ice height change, ($\bar{\mathrm{h}} = \rho b A^{-1}$), and ρ is the ice density (917 kg m^{-3}). Note that E is different from the equilibrium line altitude (ELA).

$$\mathrm{E} = (1 - \bar{\mathrm{h}})\tilde{Z} \tag{S1}$$

where $\tilde{Z}$ is the median glacial height. For every glacier we define a distribution function, $D(i)$, where i represents a grid cell of the glacier:

$$D(i) = \quad 1 - \exp\left(\frac{\left(2-\bar{\mathrm{h}}\right)(\mathrm{E}-Z(i))}{Z_{max}}\right) \tag{S2}$$

For all glaciers, is the elevation change assumed to be exponentially declining with height, $Z(i)$. The fraction in the exponential term makes sure that glaciers that on average gains up to 2 m height, will have an elevation loss in the bottom of the glacier and elevation gain at the top, unless E is equal or to Z_{max}, in which case, the whole glacier will be loosing height.

Corresponding author: Carsten Ankjær Ludwigsen, caanlu@space.dtu.dk

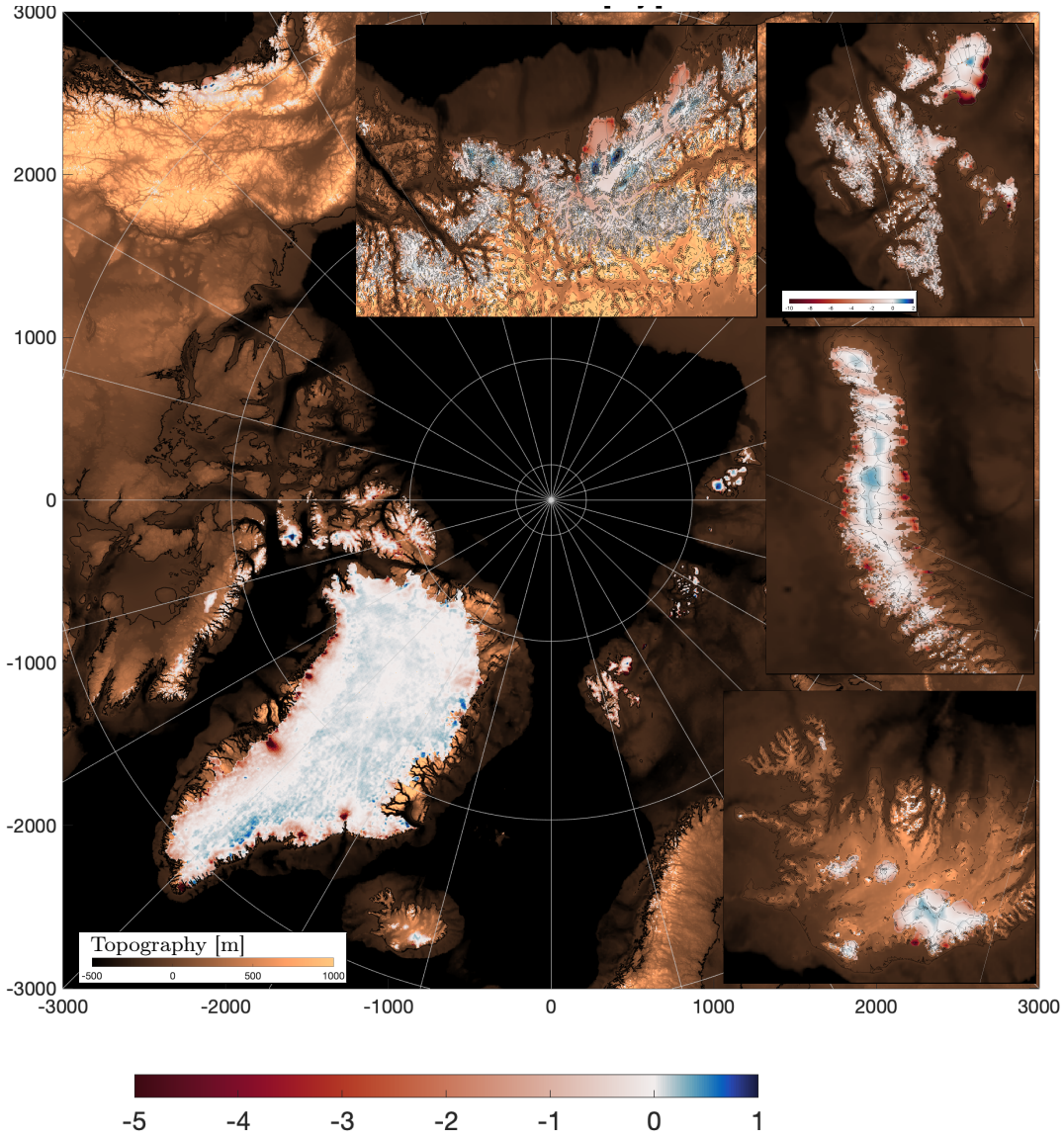

Figure S1.1. Ice elevation change from 2003 to 2015 in m yr^{-1} (red-blue scale) resulting from the redistribution explained above. The most interesting regions (Alaskian Coast, Svalbard (on a wider colorscale), Novaya Zemlja and Iceland) are enlarged. There is no significant ice loss in mainland Siberia.

The elevation change, dh/dt, is found by normalizing D, multiplying with the total mass balance, b, and converted to a height change by dividing with $\rho = 917$ kg m^{-3}.

$$\frac{dh(i)}{dt} = \frac{b}{\rho}\hat{D}(i) \qquad \text{where,} \tag{S3}$$

$$\hat{D}(i) = \frac{D(i)}{\sum_{i=1}^{k} D(i)} \tag{S4}$$

S1.1 Data availability

The ice model is available as a NetCDF-4 file on `ftp.space.dtu.dk/pub/DTU20/VLM`.

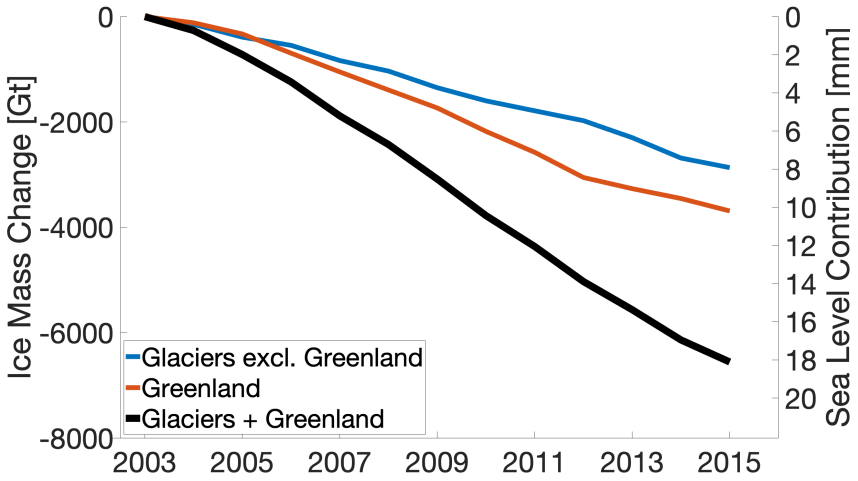

Figure S1.2. Ice loss from Greenland (including peripheral glaciers) and Arctic glaciers that goes in to the VLM calculations.

S2 Detailed description of the VLM signal at GNSS-site

In this section, we explain the VLM measured by GNSS in comparison to the VLM-model for the regions covered in this study.

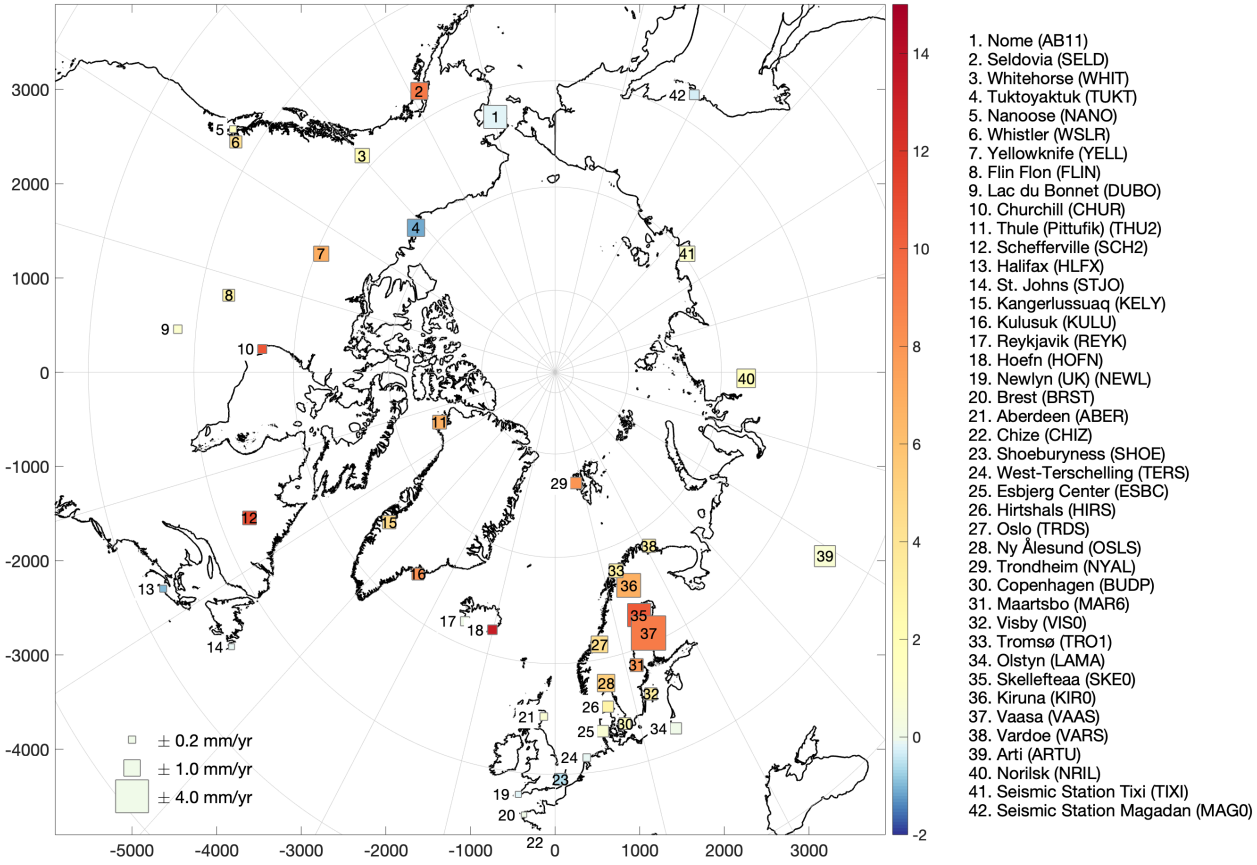

Figure S2.1. Location and name (and IGS abbreviation) of the 42 GNSS-sites used in this study ordered from most west to most east. The color indicates the linear trend from 2003-2015 [mm yr^{-1}], while the size of the square is proportional with the standard error (as estimated in the URL6-product).

S2.1 North America

The Alaskan GNSS stations show rates with opposite signs. Nome (AB11) in the Bering Strait, has a small elastic uplift which is countered by an sligthly larger GIA-caused subsidence. This results in a small total subsidence as it is also seen by the GNSS-site. Similar is the situation for Tuktoyaktuk (TUKT) where subsidience by GIA is -2.1 mm yr^{-1}, which results in a total VLM of -1.2 mm yr^{-1}, which matches the measured VLM.

The Alaska south coast which accounts for more than 25 % of the total glacial melt, is naturally dominated by elastic uplift, while GIA VLM is below 1 mm yr^{-1}. The GNSS-site Seldovia (SELD) shows large GNSS-measured uplift rates of 9.1 $\pm$ 1.1 mm yr^{-1}, while the elastic uplift rate is only 1.1 $\pm$ 0.6 mm yr^{-1} and GIA-rate -0.1 $\pm$ 0.8 mm yr^{-1}. In total this gives the second largest difference between the VLM model and GNSS VLM of the locations included in this study. Seldovia is located on the Kenai Peninsula close to the Kenai Fjords, which experienced an accelerated glacial Ice Loss in the 20th century (VanLooy et al., 2006). This is, however, not enough to explain the increased measured uplift. GIA-estimates vary in the region (Larsen et al., 2005; Hu & Freymueller, 2019), but is not more than around 1-2 mm yr^{-1}. A postseismic signal following the Prince

	IGS id	Abbr.	elastic VLM	GIA VLM	VLM-model	GNSS VLM	Model-GNSS
Nome	4	AB11	0.5 ± 0.1	-0.8 ± 0.3	-0.2 ± 0.5	-0.2 ± 2.0	-0.1 ± 2.0
Seldovia	517	SELD	1.1 ± 0.6	-0.1 ± 0.8	1.0 ± 1.3	9.1 ± 1.1	-8.2 ± 1.7
Whitehorse	651	WHIT	1.6 ± 0.8	0.9 ± 1.3	2.6 ± 2.1	2.1 ± 0.8	0.5 ± 2.2
Tuktoyaktuk	602	TUKT	0.9 ± 0.2	-2.1 ± 0.9	-1.2 ± 1.1	-1.1 ± 1.1	-0.1 ± 1.5
Nanoose	341	NANO	0.6 ± 0.3	1.5 ± 2.7	2.1 ± 3.0	1.5 ± 0.2	0.6 ± 3.0
Whistler	656	WSLR	0.9 ± 0.7	2.5 ± 3.1	3.4 ± 3.8	4.3 ± 0.5	-0.9 ± 3.8
Yellowknife	664	YELL	0.8 ± 0.2	7.6 ± 1.5	8.5 ± 1.7	6.9 ± 0.8	1.6 ± 1.9
Flin Flon	168	FLIN	0.6 ± 0.2	8.3 ± 1.6	8.9 ± 1.8	3.0 ± 0.5	5.9 ± 1.9
Lac du Bonnet	143	DUBO	0.6 ± 0.2	3.7 ± 1.1	4.3 ± 1.3	1.0 ± 0.3	3.3 ± 1.3
Churchill	106	CHUR	0.8 ± 0.3	8.4 ± 2.8	9.3 ± 3.1	10.6 ± 0.3	-1.3 ± 3.1
Thule (Pittufik)	583	THU2	5.9 ± 2.9	0.1 ± 2.1	6.0 ± 5.0	6.8 ± 0.7	-0.7 ± 5.1
Schefferville	510	SCH2	1.0 ± 0.3	15.7 ± 2.3	16.7 ± 2.6	11.0 ± 0.7	5.7 ± 2.7
Halifax	211	HLFX	0.5 ± 0.2	-1.5 ± 0.8	-1.0 ± 1.1	-1.0 ± 0.2	0.0 ± 1.1
St. Johns	548	STJO	0.7 ± 0.3	-1.4 ± 0.3	-0.7 ± 0.6	-0.1 ± 0.1	-0.5 ± 0.6
Kangerlussuaq	247	KELY	7.2 ± 3.3	2.9 ± 3.4	10.0 ± 6.6	4.7 ± 0.7	5.4 ± 6.7
Kulusuk	265	KULU	5.7 ± 1.8	-1.5 ± 1.0	4.3 ± 2.8	8.2 ± 0.5	-3.9 ± 2.9
Reykjavik	479	REYK	1.9 ± 0.5	0.2 ± 1.4	2.2 ± 2.0	0.0 ± 0.3	2.1 ± 2.0
Hoefn	215	HOFN	2.5 ± 1.0	-0.1 ± 1.0	2.3 ± 2.0	13.3 ± 0.3	-10.9 ± 2.0
Newlyn (UK)	347	NEWL	0.6 ± 0.2	-1.1 ± 0.2	-0.5 ± 0.4	-0.2 ± 0.1	-0.3 ± 0.4
Brest	72	BRST	0.5 ± 0.2	-1.0 ± 0.2	-0.5 ± 0.4	0.1 ± 0.1	-0.6 ± 0.4
Aberdeen	10	ABER	0.8 ± 0.2	-0.5 ± 0.4	0.3 ± 0.6	0.8 ± 0.2	-0.6 ± 0.7
Chize	102	CHIZ	0.4 ± 0.1	-0.3 ± 0.1	0.1 ± 0.3	0.0 ± 0.3	0.1 ± 0.4
Shoeburyness	531	SHOE	0.6 ± 0.2	-0.8 ± 0.4	-0.2 ± 0.6	-0.6 ± 0.5	0.4 ± 0.8
West-Terschelling	568	TERS	0.6 ± 0.2	-0.9 ± 0.7	-0.3 ± 0.9	-0.1 ± 0.2	-0.2 ± 0.9
Esbjerg Center	153	ESBC	0.6 ± 0.2	-0.1 ± 0.5	0.5 ± 0.7	0.8 ± 0.5	-0.2 ± 0.9
Hirtshals	210	HIRS	0.7 ± 0.2	2.2 ± 0.8	2.9 ± 1.0	2.9 ± 0.5	-0.0 ± 1.1
Oslo	596	OSLS	0.9 ± 0.2	4.6 ± 1.1	5.5 ± 1.4	4.3 ± 1.0	1.2 ± 1.7
Trondheim	370	TRDS	0.8 ± 0.2	5.0 ± 1.8	5.8 ± 2.0	5.3 ± 1.1	0.5 ± 2.3
Ny Ålesund	378	NYAL	4.9 ± 1.5	0.5 ± 0.4	5.4 ± 1.9	8.0 ± 0.5	-2.6 ± 2.0
Copenhagen	75	BUDP	0.6 ± 0.2	0.9 ± 0.5	1.5 ± 0.6	1.7 ± 0.5	-0.2 ± 0.8
Maartsbo	306	MAR6	0.7 ± 0.2	7.6 ± 2.4	8.3 ± 2.6	8.0 ± 0.6	0.3 ± 2.7
Visby	639	VIS0	0.6 ± 0.2	3.3 ± 1.1	3.9 ± 1.3	3.4 ± 0.6	0.5 ± 1.4
Tromsø	599	TRO1	1.0 ± 0.3	1.7 ± 0.7	2.7 ± 0.9	3.1 ± 0.7	-0.4 ± 1.2
Olstyn	274	LAMA	0.5 ± 0.1	0.1 ± 0.5	0.6 ± 0.7	0.0 ± 0.5	0.5 ± 0.8
Skellefteaa	534	SKE0	0.8 ± 0.2	8.5 ± 2.1	9.3 ± 2.3	10.4 ± 2.0	-1.0 ± 3.1
Kiruna	252	KIR0	0.9 ± 0.3	5.2 ± 0.9	6.1 ± 1.1	6.8 ± 2.1	-0.7 ± 2.4
Vaasa	625	VAAS	0.7 ± 0.2	8.3 ± 2.2	9.0 ± 2.4	9.1 ± 4.4	-0.1 ± 5.0
Vardoe	630	VARS	0.9 ± 0.3	2.0 ± 0.6	2.9 ± 0.8	3.1 ± 0.6	-0.1 ± 1.1
Arti	36	ARTU	0.2 ± 0.1	-0.2 ± 0.2	-0.0 ± 0.3	0.8 ± 1.6	-0.8 ± 1.7
Norilsk	360	NRIL	0.5 ± 0.2	1.9 ± 0.2	2.4 ± 0.4	1.8 ± 1.3	0.6 ± 1.3
Seismic Station Tixi	587	TIXI	0.5 ± 0.1	-0.3 ± 0.3	0.1 ± 0.4	1.0 ± 0.9	-0.9 ± 1.0
Seismic Station Magadan	298	MAG0	0.2 ± 0.1	-0.2 ± 0.2	-0.0 ± 0.2	-0.3 ± 0.3	0.3 ± 0.4

Table S2.1. Measured and modelled VLM for each GNSS-site in mm yr^{-1}. VLM-model is the sum of elastic VLM and GIA VLM.

Willam Sound Earthquake in 1964 explained by Cohen and Freymueller (2001) is still causing a locally increased uplift on this side of the peninsula. Our study indicate this effect to be 8.2 mm yr^{-1} from 2003-2015, which roughly matches the study by Cohen and Freymueller (2001), where they find the post seismic uplift to be 9.3 mm yr^{-1} from 1994-2001. This rebound is expected to decay further over time, but will still be relevant for decades to come (Cohen & Freymueller, 2001).

Whitehorse, Nanoose and Whistler, are dominated by large GIA-uncertainties, which are larger than the VLM-signal itself and 3-4 times larger than the residual between the VLM model and GNSS VLM. Yellowknife (YELL), Flin Flon (FLIN) and Lac du Bonnet (DUBO) are at the periphery of the largest GIA-rate, but have no large nearby glaciers to cause significant elastic uplifts. It is an area known to have uncertain GIA-estimates, e.g. does the ICE6G-model (Peltier et al., 2015) have lower GIA-rates in better alignment with the measured GNSS VLM. The same residuals are also seen by Frederikse et al. (2019), which uses the same GIA model (Caron2018). The VLM predictions for Churchill

(CHUR) at the south-east coast of Hudson Bay, is in good alignment with the GNSS-measured VLM, while the deformationen rate for Schefferville (SCH2) also is overestimated in the model.

At the Canadian Atlantic coast is GIA causing a subsidence. The VLM model shows, that a smaller positive elastic deformation is mitigating the subsidence, which in total gives a rate in the order of -1 mm yr^{-1}, which agrees well with GNSS VLM measured at Halifax, Nova Scotia (HLFX) and St. Johns, New Foundland (STJO).

S2.2 Iceland

The two GNSS-sites in this study show very different uplift rates of 0.0 ± 0.3 mm yr^{-1} in Reykjavik (REYK) and 13.3 ± 0.3 mm yr^{-1} at Hoefn (HOFN) at the southnern edge of the largest ice cap on Iceland, Vatnajökull. The VLM-model overestimates the rebound in Reykjavik while it largely underestimates it at Hoefn. A probable explanation for this is the thin crustal layer and a soft viscoelastic mantly layer (Fleming et al., 2007), which creates a present-day viscoelastic signal that is much larger than the ones predicted by the GIA-model or in the 1-D earth rheology included in the elastic VLM-calculations (Sørensen et al., 2017). A thin crust, also means that the uplift decreases faster with distance to the glacier (Fleming et al., 2007), which could explain why Reykjavik shows little vertical deformation.

S2.3 Svalbard

The majority of land in Svalbard is covered with ice, and vertical deformation highly influenced by ongoing ice-mass changes. The only site from Svalbard included in this study is Ny Ålesund (NYAL), which is located on the west coast. At this location, the VLM-model is dominated by an elastic uplift of 4.9 ± 1.5 mm yr^{-1} and GIA of 0.5± 0.4 mm yr^{-1}. In total this is 2.6 mm yr^{-1} short of the measured GNSS VLM. While global GIA-models agree within ± 0.2 mm yr^{-1}, more focused, but older studies predict a slightly higher GIA contribution of around 1.5 mm yr^{-1} (Sato et al., 2006; Kierulf et al., 2009). Another contribution to VLM, which is relevant for VLM-studies in glaciated regions, is the 'short-term mantle memory', (Mémin et al., 2014; Rajner, 2018), which is a non-instant relaxation of the mantle after being depressed by an load. Svalbard likely experienced significant deglaciation after the little ice age (LIA) that ended in the end of the 19th century (Grove, 2001). The effect is quite uncertain (Rajner, 2018) and Mémin et al. (2014) estimated the post-LIA rebound to be 2-5 mm yr^{-1} in the beginning of 21st century, which would explain the residual of 2.6 mm yr^{-1}.

S2.4 Northern Europe and Scandinavia

The fennoscandinavian icecap from the last ice ages is causing a GIA that is dominating the vertical deformation in Scandinavia (figure 1). Even though small glaciers exist in particular Norway, the elastic effect is very local and has almost negligible effect on the GNSS-sites in this study. The contour lines of the elastic rebound are clearly parallel to Greenland (figure 1), which indicates, that the wavelength of the elastic VLM of Greenland is determining the elastic VLM in Scandinavia and Northern Europe.

GIA is around 3-5 times larger than the elastic VLM in most of Scandinavia. However it is clear, that for many of the GNSS-sites, can the VLM-signal only be explained by combining the elastic VLM model with GIA. This becomes more prominent for GNSS-sites in areas, where GIA is less dominant. Esbjerg (ESBC) on the west coast of Denmark is close to the zero-line of the GIA VLM, but is still measuring an uplift of about 0.8 mm yr^{-1}. The VLM-model predicts elastic uplift rates of about 0.6 ± 0.2 mm yr^{-1}, which agrees with the GNSS VLM. South of the zero-line in Northern Europe, where the

GIA-rate is negative, the elastic VLM caused by present day ice melt, is somewhat mitigating the subsidence, which is also seen along the North American east coast.

S2.5 Siberia

Only a few available GNSS measurements exist in eastern Europe and Siberia. The GIA-model by Caron et al. (2018) is also challenged by limited resources of paleo sea-level records, which makes the GIA-model more dependent on the existing GNSS-records. It is commonly anticipated that Siberia had little or no ice during the last glacial cycle (Whitehouse et al., 2007), except some ice in the north central Siberia and in the shallow waters in the Barents Sea between Svalbard and Novaya Zemlya (Root et al., 2015). The old ICE3G GIA model by Tushingham and Peltier (1991) contained included some prehistoric ice over the western Siberia, which disappeared in the later version ICE5G and ICE6G (Peltier et al., 2015).

Also the Elastic uplift is limited in the region, with values around 0.5 mm yr^{-1}. While the GNSS VLM is within in the error-range of the modelled VLM for the Siberian GNSS-sites (Arti (ARTU), Norilsk (NRIL), Tixi (TIXI) and Magadan (MAG0)), it seems that a GIA-only model would better fit the GNSS measurements, which possibly is because of the enhanced GNSS-dependency of the GIA-model.

S3 Timeseries of vertical deformation at all GNSS sites

Figure S3.1 shows both measured and modeled vertical deformation from 2003-2015 of each individual GNSS-site. It also reflects, how elastic VLM is changing year by year, while GIA is linear.

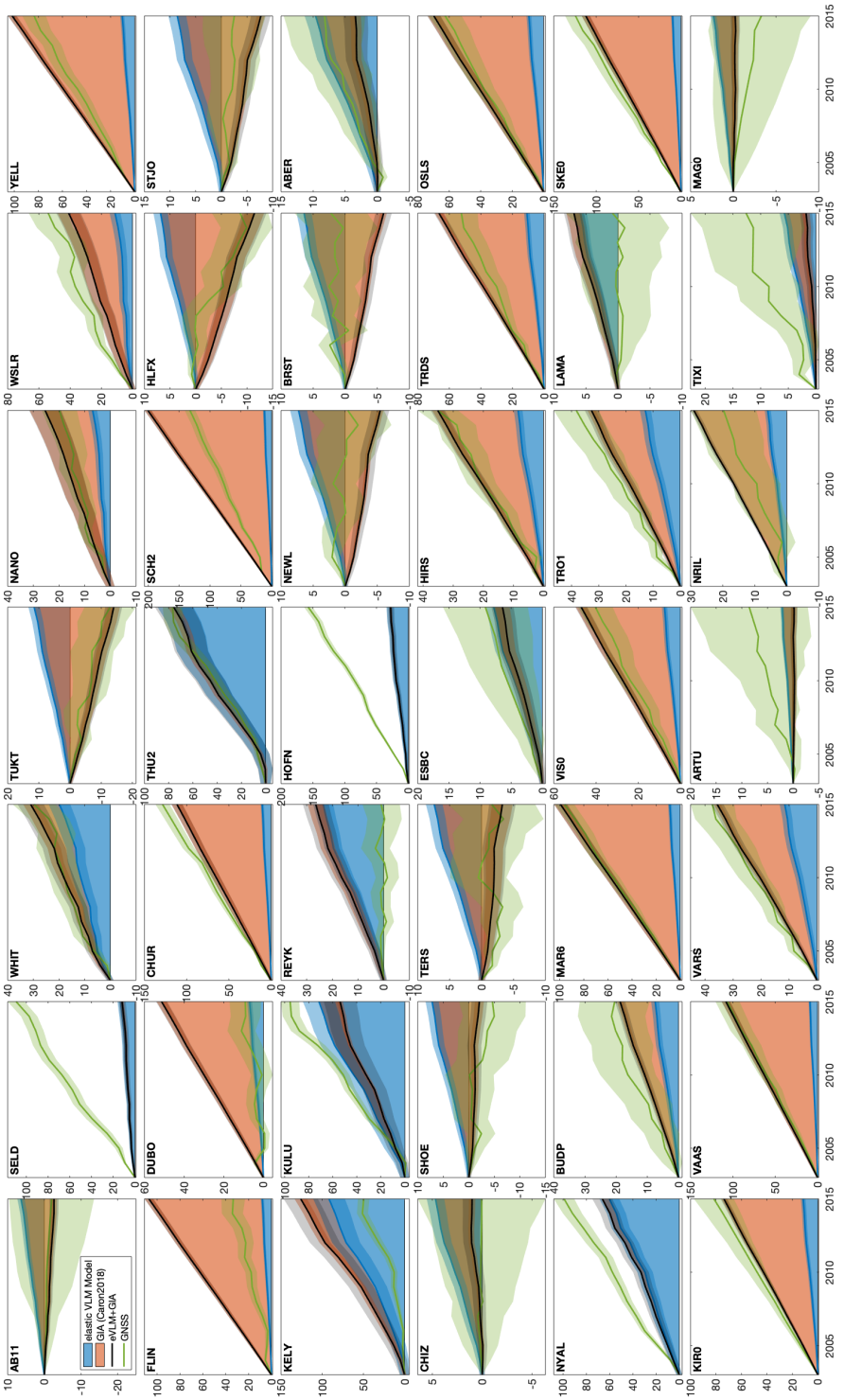

Figure S3.1. Measured and predicted vertical deformation from 2003 to 2015 for the 42 GNSS locations. GNSS is shown by the green line (green shadow denotes the error range) and the VLM model by the black line (error range is shown by the grey area). The red and blue areas indicate the part of the VLM model that is elastic and GIA.

References

Caron, L., Ivins, E. R., Larour, E., Adhikari, S., Nilsson, J., & Blewitt, G. (2018). Gia model statistics for grace hydrology, cryosphere, and ocean science. *Geophysical Research Letters*, *45*(5), 2203-2212. Retrieved from https://agupubs.onlinelibrary.wiley.com/doi/abs/10.1002/2017GL076644 doi: 10.1002/2017GL076644

Cohen, S. C., & Freymueller, J. T. (2001). Crustal uplift in the south central alaska subduction zone: New analysis and interpretation of tide gauge observations. *Journal of Geophysical Research: Solid Earth*, *106*(B6), 11259-11270. Retrieved from https://agupubs.onlinelibrary.wiley.com/doi/abs/10.1029/2000JB900419 doi: 10.1029/2000JB900419

Fleming, K., Martinec, Z., & Wolf, D. (2007, 01). Glacial-isostatic adjustment and the viscosity structure underlying the vatnajökull ice cap, iceland. *Pure and Applied Geophysics*, *164*, 751-768. doi: 10.1007/s00024-007-0187-6

Frederikse, T., Landerer, F. W., & Caron, L. (2019). The imprints of contemporary mass redistribution on local sea level and vertical land motion observations. *Solid Earth*, *10*(6), 1971–1987. Retrieved from https://www.solid-earth.net/10/1971/2019/ doi: 10.5194/se-10-1971-2019

Grove, J. (2001, 01). The initiation of the "little ice age" in regions round the north atlantic. *Climatic Change*, *48*, 53-82. doi: 10.1023/A:1005662822136

Hu, Y., & Freymueller, J. T. (2019). Geodetic observations of time-variable glacial isostatic adjustment in southeast alaska and its implications for earth rheology. *Journal of Geophysical Research: Solid Earth*, *124*(9), 9870-9889. Retrieved from https://agupubs.onlinelibrary.wiley.com/doi/abs/10.1029/2018JB017028 doi: 10.1029/2018JB017028

Kierulf, H. P., Plag, H.-P., & Kohler, J. (2009, 10). Surface deformation induced by present-day ice melting in Svalbard. *Geophysical Journal International*, *179*(1), 1-13. Retrieved from https://doi.org/10.1111/j.1365-246X.2009.04322.x doi: 10.1111/j.1365-246X.2009.04322.x

Larsen, C. F., Motyka, R. J., Freymueller, J. T., Echelmeyer, K. A., & Ivins, E. R. (2005). Rapid viscoelastic uplift in southeast alaska caused by post-little ice age glacial retreat. *Earth and Planetary Science Letters*, *237*(3), 548 - 560. Retrieved from http://www.sciencedirect.com/science/article/pii/S0012821X05004152 doi: https://doi.org/10.1016/j.epsl.2005.06.032

Mémin, A., Spada, G., Boy, J.-P., Rogister, Y., & Hinderer, J. (2014, 05). Decadal geodetic variations in Ny-Ålesund (Svalbard): role of past and present ice-mass changes . *Geophysical Journal International*, *198*(1), 285-297. Retrieved from https://doi.org/10.1093/gji/ggu134 doi: 10.1093/gji/ggu134

Peltier, W., Argus, D., & Drummond, R. (2015). Space geodesy constrains ice age terminal deglaciation: The global ice-6g-c (vm5a) model. *Journal of Geophysical Research: Solid Earth*, *120*(1), 450-487. Retrieved from https://www.scopus.com/inward/record.uri?eid=2-s2.0-85027948080&doi=10.1002%2f2014JB011176&partnerID=40&md5=29a7ce38c5cf3872d2276981d2f6b34f (cited By 326) doi: 10.1002/2014JB011176

Pfeffer, W. T., Arendt, A. A., Bliss, A., Bolch, T., Cogley, J. G., Gardner, A. S., ... et al. (2014). The randolph glacier inventory: a globally complete inventory of glaciers. *Journal of Glaciology*, *60*(221), 537–552. doi: 10.3189/2014JoG13J176

Rajner, M. (2018). Detection of ice mass variation using gnss measurements at svalbard. *Journal of Geodynamics*, *121*, 20 - 25. Retrieved from http://www.sciencedirect.com/science/article/pii/S0264370718300450 doi: https://doi.org/10.1016/j.jog.2018.06.001

Root, B. C., Tarasov, L., & van der Wal, W. (2015). Grace gravity observations constrain weichselian ice thickness in the barents sea. *Geophysical Research Letters*, *42*(9), 3313-3320. Retrieved from https://agupubs.onlinelibrary

.wiley.com/doi/abs/10.1002/2015GL063769 doi: 10.1002/2015GL063769

Sato, T., Okuno, J., Hinderer, J., MacMillan, D. S., Plag, H.-P., Francis, O., ... Fukuda, Y. (2006, 06). A geophysical interpretation of the secular displacement and gravity rates observed at Ny-Ålesund, Svalbard in the Arctic—effects of post-glacial rebound and present-day ice melting. *Geophysical Journal International*, *165*(3), 729-743. Retrieved from https://doi.org/10.1111/j.1365-246X.2006.02992.x doi: 10.1111/j.1365-246X.2006.02992.x

Sørensen, L. S., Jarosch, A. H., Adalgeirsdóttir, G., Barletta, V. R., Forsberg, R., Pálsson, F., ... Jóhannesson, T. (2017, 01). The effect of signal leakage and glacial isostatic rebound on GRACE-derived ice mass changes in Iceland. *Geophysical Journal International*, *209*(1), 226-233. Retrieved from https://doi.org/10.1093/gji/ggx008 doi: 10.1093/gji/ggx008

Tushingham, A. M., & Peltier, W. R. (1991). Ice-3g: A new global model of late pleistocene deglaciation based upon geophysical predictions of post-glacial relative sea level change. *Journal of Geophysical Research: Solid Earth*, *96*(B3), 4497-4523. Retrieved from https://agupubs.onlinelibrary.wiley.com/doi/abs/10.1029/90JB01583 doi: 10.1029/90JB01583

VanLooy, J., Forster, R., & Ford, A. (2006). Accelerating thinning of kenai peninsula glaciers, alaska. *Geophysical Research Letters*, *33*(21). Retrieved from https://agupubs.onlinelibrary.wiley.com/doi/abs/10.1029/2006GL028060 doi: 10.1029/2006GL028060

Whitehouse, P. L., Allen, M. B., & Milne, G. A. (2007, 08). Glacial isostatic adjustment as a control on coastal processes: An example from the Siberian Arctic. *Geology*, *35*(8), 747-750. Retrieved from https://doi.org/10.1130/G23437A.1 doi: 10.1130/G23437A.1